[1] L. Addadi, S. Weiner, in *Biomineralization: Chemical and Biochemical Perspectives* (Eds: S. Mann, J. Webb, R. J. P. Williams), VCH, Weinheim, Germany **1989**, Ch. 5.
[2] S. Mann, *Biomineralization: Principles and Concepts in Bioinorganic Materials Chemistry*, Oxford University Press, Oxford, UK **2001**.
[3] M. Fritz, A. M. Belcher, M. Radmacher, D. A. Walters, P. K. Hansma, G. D. Stucky, D. E. Morse, S. Mann, *Nature* **1994**, *371*, 49.
[4] S. R. Qiu, A. Wierzbicki, C. A. Orme, A. M. Cody, J. R. Hoyer, G. H. Nancollas, S. Zepeda, J. J. De Yoreo, *Proc. Natl. Acad. Sci. USA* **2004**, *101*, 1793.
[5] H. H. Teng, P. M. Dove, J. J. De Yoreo, *Geochim. Cosmochim. Acta* **1999**, *63*, 2507.
[6] C. A. Orme, A. Noy, A. Wierzbicki, M. T. McBride, M. Grantham, H. H. Teng, P. M. Dove, J. J. De Yoreo, *Nature* **2001**, *411*, 775.
[7] S. Geider, A. Baronnet, C. Cerini, S. Nitsche, J. P. Astier, R. Michel, R. Boistelle, Y. Berland, J. C. Dagorn, J. M. Verdier, *J. Biol. Chem.* **1996**, *271*, 26 302.
[8] A. Berman, L. Addadi, S. Weiner, *Nature* **1988**, *331*, 546.
[9] K. J. Davis, P. M. Dove, J. J. De Yoreo, *Science* **2000**, *290*, 1134.
[10] L. E. Wasylenki, P. M. Dove, D. S. Wilson, J. J. De Yoreo, *Geochim. Cosmochim. Acta* **2005**, *69*, 3017.
[11] K. J. Davis, P. M. Dove, L. E. Wasylenki, J. J. De Yoreo, *Am. Mineral.* **2004**, *89*, 714.
[12] S. Elhadj, N. Han, P. M. Dove, E. Salter, A. Wierzbicki, J. J. De Yoreo, *EOS Trans. AGU* **2004**, *85*, B21B-0871.
[13] G. Fu, S. Valiyaveettil, B. Wopenka, D. E. Morse, *Biomacromolecules* **2005**, *6*, 1289.
[14] J. J. De Yoreo, P. G. Vekilov, in *Biomineralization*, Vol. 54 (Eds: P. M. Dove, J. J. De Yoreo, S. Weiner), The Mineralogical Society of America, Washington, DC **2003**, p. 57.
[15] P. M. Dove, J. J. De Yoreo, K. J. Davis, in *Nanoscale Structure and Assembly at Solid–Fluid Interfaces*, Vol. 2 (Eds: X. Y. Liu, J. J. De Yoreo), Kluwer Academic, New York **2004**, p. 55.
[16] D. A. Walters, B. L. Smith, A. M. Belcher, G. T. Paloczi, G. D. Stucky, D. E. Morse, P. K. Hansma, *Biophys. J.* **1997**, *72*, 1425.
[17] N. Sreerama, R. W. Woody, *Anal. Biochem.* **2000**, *287*, 252.
[18] M. Michenfelder, G. Fu, C. Lawrence, J. C. Weaver, B. A. Wustman, L. Taranto, J. S. Evans, D. E. Morse, *Biopolymers* **2003**, *70*, 522.
[19] J. S. Evans, S. I. Chan, W. A. Goddard, *Protein Sci.* **1995**, *4*, 2019.
[20] S. Weiner, L. Addadi, *Trends Biochem. Sci.* **1991**, *16*, 252.
[21] D. W. P. M. Luwik, J. C. M. van Hest, *Chem. Soc. Rev.* **2004**, *33*, 234.
[22] Q. Q. Hoang, F. Sicheri, A. J. Howard, D. S. C. Yang, *Nature* **2003**, *425*, 977.
[23] J. Baardsnes, L. H. Kondejewski, R. S. Hodges, H. Chao, C. Kay, P. L. Davies, *FEBS Lett.* **1999**, *463*, 87.
[24] B.-A. Gotliv, N. Kessler, J. L. Sumerel, D. E. Morse, N. Tuross, L. Addadi, S. Weiner, *ChemBioChem* **2005**, *6*, 304.
[25] S. Mann, J. M. Didymus, N. P. Sanderson, B. R. Heywood, *J. Chem. Soc., Faraday Trans.* **1990**, *86*, 1873.
[26] D. B. DeOliveira, R. A. Laursen, *J. Am. Chem. Soc.* **1997**, *119*, 10 627.
[27] Y.-J. Han, J. Aizenberg, *J. Am. Chem. Soc.* **2003**, *125*, 4032.
[28] T. A. Land, J. J. De Yoreo, J. D. Lee, *Surf. Sci.* **1997**, *384*, 136.
[29] S. Brahms, J. Brahms, *J. Mol. Biol.* **1980**, *138*, 149.
[30] B. R. Baker, R. L. Garrell, *Faraday Discuss.* **2004**, *126*, 209.
[31] D. K. Wilkins, S. B. Grimshaw, V. Receveur, C. M. Dobson, J. A. Jones, L. J. Smith, *Biochemistry* **1999**, *38*, 16 424.

Magnetic Nanocrescents as Controllable Surface-Enhanced Raman Scattering Nanoprobes for Biomolecular Imaging**

By *Gang L. Liu*, *Yu Lu*, *Jaeyoun Kim*, *Joseph C. Doll*, and *Luke P. Lee**

Surface-enhanced Raman scattering (SERS) spectroscopy shows chemical-bond information, and it is one of the best methods for label-free biomolecular imaging. Conventional SERS substrates require multiple plasmonic couplings via many colloidal nanoparticles, and it is difficult to control the coupling distance. Here, we report the design, fabrication, and characterization of a biocompatible composite (Au/Ag/Fe/Au) nanocrescent SERS nanoprobe, which can not only function as a standalone SERS substrate with integrated SERS hot-spot geometries, but can also be controlled magnetically to produce orientational and translational motions. A single nanocrescent demonstrates a SERS enhancement factor higher than 10^8 in the detection of sub-zeptomole molecular concentrations. Magnetically modulated SERS detection of molecules on a single composite nanocrescent probe is demonstrated. The gold surfaces of composite nanocrescent SERS probes are biocompatible, and thus they can be biofunctionalized and applied in real-time biomolecular imaging.

Unlike conventional fluorescence imaging, Raman spectroscopy acquires unique signatures of chemical and biological molecules without labeling with fluorophore molecules.[1] Raman imaging of living cells can nondestructively probe the intracellular biochemical dynamics without prior fluorescent or radioactive labeling,[2] but the formidably low efficiency of Raman scattering hinders its applications in the detection of molecules at micromolar or lower concentrations. However, SERS by metallic nanostructures increases the original Raman scattering intensity for many orders of magnitude, which makes the Raman detection of low concentration molecules practical.[3] Colloidal Au or Ag nanoparticle clusters are commonly used as SERS substrates, and Raman enhancement factors as high as 10^{14} have been reported in single-molecular-

[*] Prof. L. P. Lee, G. L. Liu, Dr. Y. Lu, Dr. J. Kim, J. C. Doll
Biomolecular Nanotechnology Center and
Berkeley Sensor and Actuator Center
Department of Bioengineering, University of California-Berkeley
Berkeley, CA 94720 (USA)
E-mail: lplee@berkeley.edu

[**] We appreciate Dr. Y. Yin and Prof. A. P. Alivisatos in the Molecular Foundry at the Lawrence Berkeley National Laboratory for assistance with TEM imaging. This work is supported by DARPA and Samsung Electronics. J. K. was supported by a grant (05K1501-02810) from the Center for Nanostructured Materials Technology under 21st Century Frontier R&D Programs of the Ministry of Science and Technology, Korea. Supporting Information is available online from Wiley InterScience or from the author.

 DOI: 10.1002/adma.200501064

ADVANCED MATERIALS

level detections.[4,5] Au and Ag nanoparticles are also utilized in Raman cellular imaging to enhance signal intensity and increase image contrast.[6] However, conventional nanoparticles have inherent limits for in-vivo biomolecular SERS imaging in that 1) strong Raman enhancement relies on good coupling between adjacent nanoparticles, so called "hot spots", which is inconsistent for randomly formed nanoparticle clusters; 2) the spatial imaging resolution degrades with increasing size of nanoparticles clusters; and 3) the random distribution of nanoparticles within the biological cell voids the spatial specificity. We have previously developed Au nanocrescent structures with sub-10 nm sharp edges that can be used as excellent standalone SERS probes.[7] In comparison with other available single-nanoparticle-based SERS substrates, such as nanoshells,[8] nanotips,[9] and nanorings,[10] the Au nanocrescent has a higher local field-enhancement factor in the near-infrared wavelength region due to the simultaneous incorporation of SERS hot spots including sharp nanotip and nanoring geometries, leading to the strong hybrid resonance modes from nanocavity resonance modes and tip–tip intercoupling modes. However, the previously demonstrated Au nanocrescent is inconvenient in practical applications, and especially intracellular SERS sensing, because the orientation and position of the gold nanocrescents are random. In fact, controllable micro- or nanoparticles have been extensively used in biomolecular and cellular sensing by means of magnetic, electric, or optical control schemes. Magnetically modulated fluorescent microparticles were demonstrated to achieve higher signal-to-noise ratios in fluorescence imaging.[11]

In this communication, we report magnetically controllable nanocrescent SERS probes by incorporating composite layers with a ferromagnetic material (Fig. 1a). Nanostructured composite multilayer design (Au/Ag/Fe/Au) with magnetic thin film allows an ideal biophotonic molecular probe controllable with an external magnetic field. The fabrication process of a composite nanocrescent (see Fig. S1 in the Supporting Information) is similar to that reported previously,[7] here forming a multilayer of 10 nm Au, 10 nm Fe, 20 nm Ag, and 10 nm Au. Details of fabrication are described in the Experimental section. The choice of materials and multilayer thickness are intentionally designed with the assistance of finite-element simulation in order to tune the plasmon-resonance wavelength of the composite nanocrescent matched with the excitation wavelength. The nanocrescent has a sub-10 nm sharp

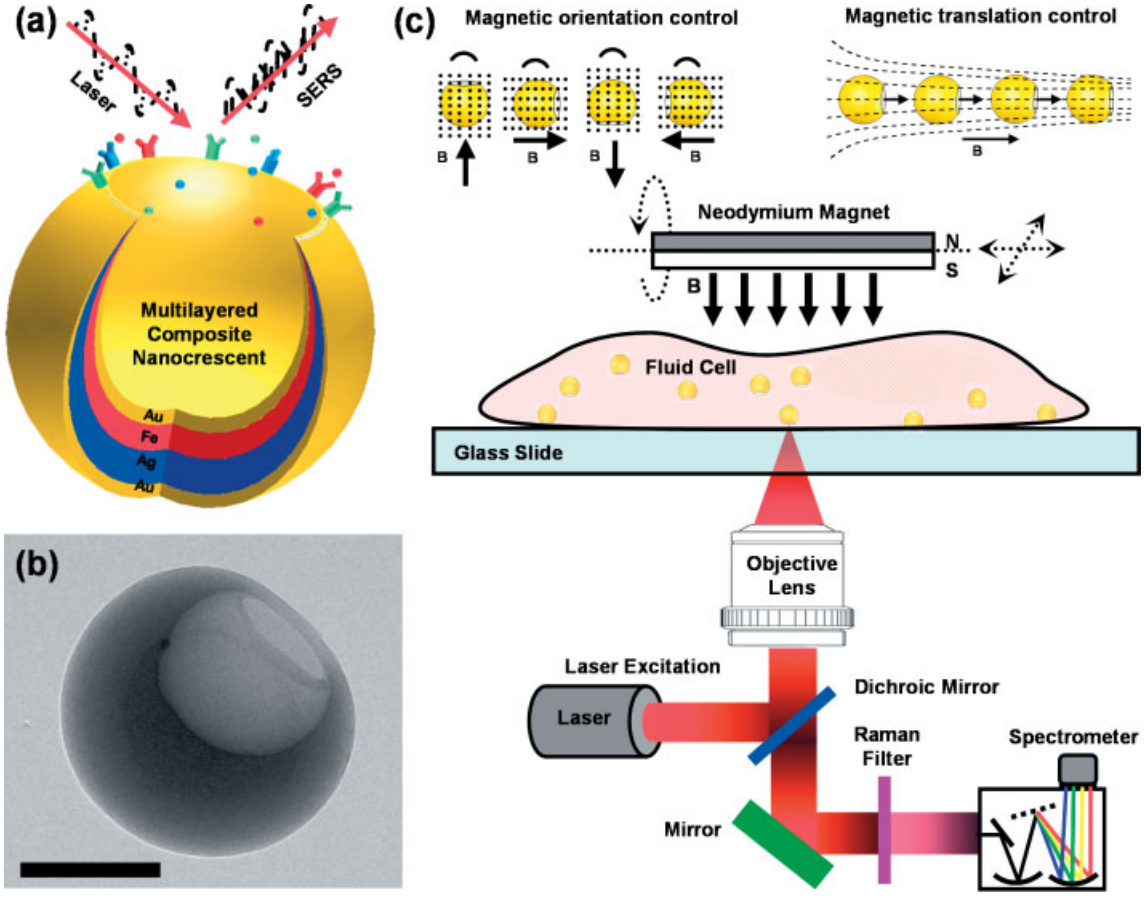

Figure 1. Composite material magnetic nanocrescent SERS probes. a) Schematic diagram of SERS detection on a single composite nanocrescent. b) Transmission electron microscopy image of a single magnetic nanocrescent SERS probe. The scale bar represents 100 nm. c) Schematic diagram of a SERS imaging system and the magnetic manipulation system for intracellular biomolecular imaging (in fluids) using standalone magnetic nanocrescent SERS probes.

edge, although the multilayer structure is not clearly distinguishable in the transmission electron microscopy (TEM) image (Fig. 1b) due to the low imaging contrast between the different metallic materials of Au, Ag, and Fe. The nanocrescents suspended in the fluids are then controlled by magnetic fields during the SERS imaging (Fig. 1c).

In addition to magnetostatic force, the reduced-symmetry geometrical shape of the nanocrescents enables net torque to be generated by an external magnetic field (Fig. S2). Hence, the nanocrescent can be both moved and oriented by controlling the external magnetic field. To observe the responses of nanocrescents to magnetic modulation, some nanocrescents were intentionally fabricated using fluorescent polystyrene nanosphere templates (150 nm in diameter). In this case, we used the fluorescent polystyrene nanosphere template without removing it, which enables the use of an epifluorescence video microscopy system in tracking the movements of the nanocrescents at high speeds during the magnetic manipulation. A neodymium permanent magnet is mounted in a close proximity above a closed microfluidic cell with nanocrescents suspended in liquid. By rotating the permanent magnet at a frequency of 0.5 Hz and varying the orientation of the magnetic field, the orientation and fluorescence intensity of the fluorescent nanocrescents can be modulated as shown in Figure 2a. The fluorescence intensity is higher when the excitation light directly impinges on the fluorescent nanosphere, while the fluorescence intensity is lower when the metallic multilayer blocks the excitation light path. Due to the thermal tumbling of the nanocrescent and the slight change of magnetic field component in the lateral direction, jitters in the modulated fluorescent signal can be observed, but the position of the nanocrescent remains within a ~3 μm × 3 μm square area during the rotation process. Figure 2b shows the lateral translation of a single fluorescent nanocrescent controlled by the permanent magnet. The sequential image frames are taken every half second during the lateral movement of the nanocrescent. The lateral motions of the nanocrescents are limited to a certain image plane (variation within vertical resolution of the 40× objective lens are ~10 μm) due to the balance between gravity, buoyancy, drag, and the magnetic force in the vertical direction, although the magnetic-field component in the vertical direction slightly changes during the lateral motion of the permanent magnet. We found the vertical motion of nanocrescents is much more insensitive to magnetic actuations than lateral motion.

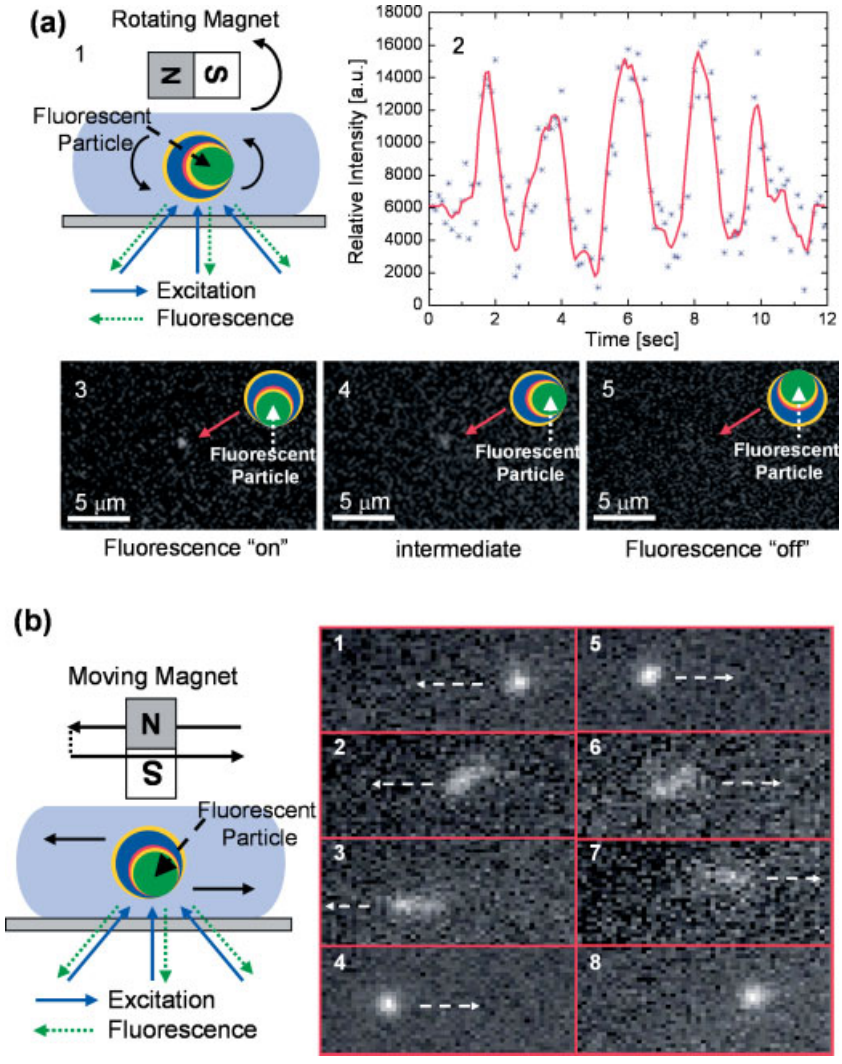

Figure 2. Magnetic manipulation of a single nanocrescent attached to a fluorescent polystyrene nanosphere. a) Magnetically modulated rotation of a single nanocrescent. 1) Schematic diagram of the experimental setup. The orientation of the nanocrescent follows the rotation of the permanent magnet at the frequency of 0.5 Hz. 2) Modulated fluorescence intensity of the nanocrescent as a function of time; 3–5) Representative images of the nanocrescent with different orientations when the fluorescence intensity is maximal (3), minimal (5), and intermediate (4). b) Schematic diagram and fluorescence images of the magnetically modulated lateral translation of a single fluorescent nanocrescent. Frames 1–8 are representative images taken with a 0.5 s time interval showing how the single fluorescent nanosphere is moved back and forth horizontally by moving the magnet.

In contrast to spherical metallic nanoparticles, the nanocrescents have plasmon resonance modes in the near-infrared wavelength region and a much higher local field enhancement (~20 dB of electric-field amplitude). However, the enhancement factor and local field distribution are dependent on the orientation of the nanocrescents with respect to the incident direction of excitation light, as shown in the finite element simulation (Fig. 3a). We used FEMLAB electromagnetic sim-

ADVANCED MATERIALS

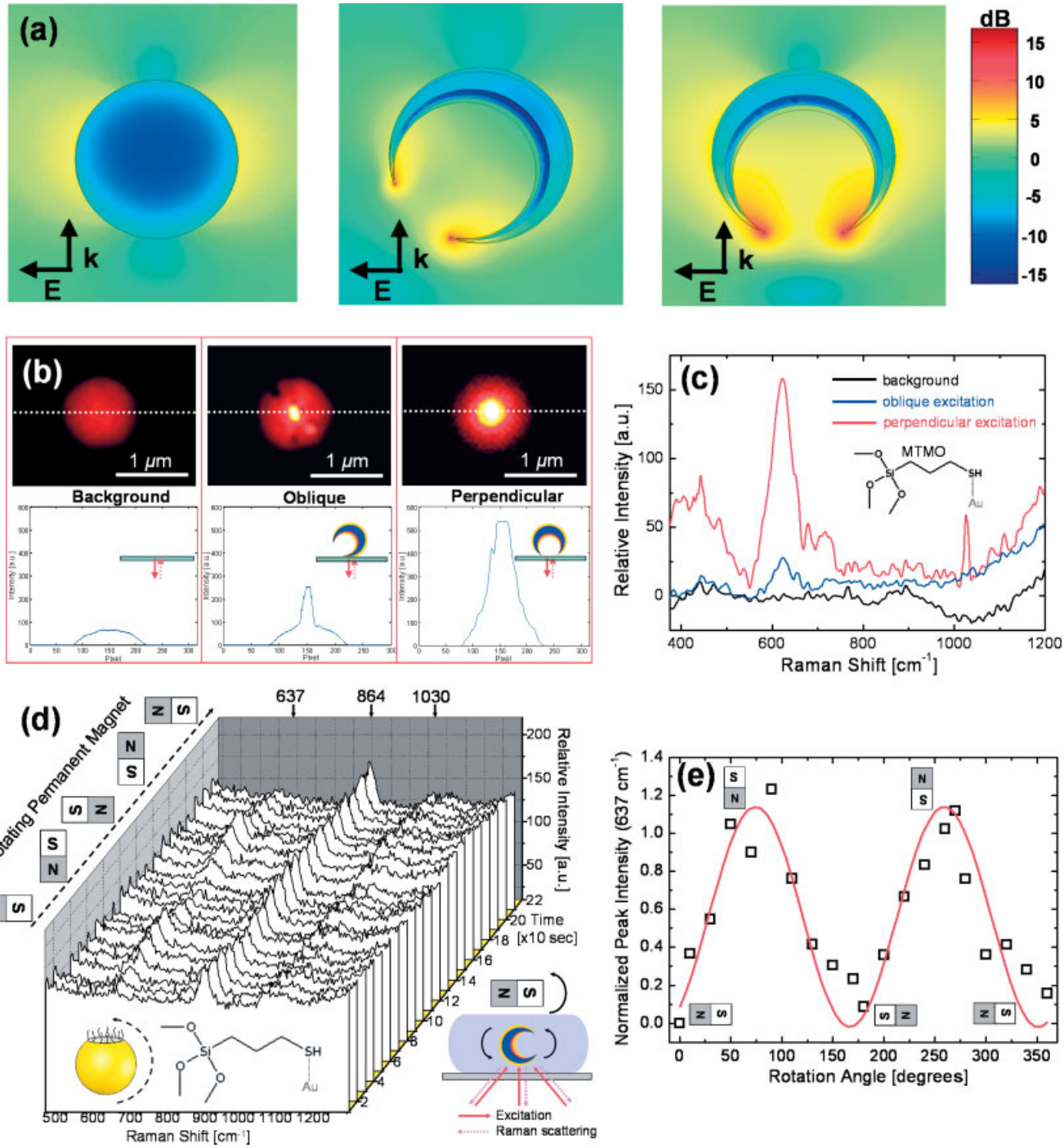

Figure 3. Magnetically modulated SERS detection of 3-mercaptopropyltrimethoxysilane (MTMO) molecules tethered on a single nanocrescent. a) Simulated local electric-field-amplitude enhancement in dB by a single nanocrescent oriented 0° (right) and 45° (middle) with respect to the 785 nm light-incident direction, in comparison with an 80 nm Au nanosphere (left). b) Intensity images and the cross-line intensity plots of a laser focal spot without a nanocrescent (left), and with a single nanocrescent obliquely (middle) and perpendicularly (right) oriented with respect to the direction of excitation laser light. c) SERS spectra of MTMO molecules on the surface of the glass slide (background), and on the single nanocrescents with oblique and perpendicular orientations. d) Series of SERS spectra as a function of time while continuously changing the external magnetic field direction. e) Intensity plot of the 637 cm^{-1} Raman peak versus approximate rotational angles of the permanent magnet.

ulation software (COMSOL, CA) to generate the results. The maximum local field enhancement is achieved when the propagation direction of the excitation field is parallel to the symmetry line of the nanocrescents. In an experiment, a circularly polarized near-infrared laser (785 nm) is focused on the nanoparticles by a high numerical aperture (NA) microscopy ob-

jective lens. No optical filter is used in this measurement. The local field intensity measured from the far field shows that the enhancement by a single nanocrescent, shown in the right image of Figure 3b, is greater than fivefold, which cannot be attributed to reflections from the metallic surface, because reflection becomes negligible and scattering dominates for structures much smaller than the excitation wavelength. In contrast, another nanocrescent, shown in the middle image of Figure 3b, only generates a two- to threefold enhancement, possibly due to a different orientation, which verifies that the local field enhancement of the composite nanocrescents depends on their orientations. The inset drawings in Figure 3b illustrate the possible orientations of these two nanocrescents, and the cross-line intensity plots further clarify the orientation-dependent field enhancement effect. 80 nm Au nanospheres (not shown) were also tested, but no significant field-enhancement effect was observed at the 785 nm excitation wavelength.

We also compare the SERS spectra of chemical molecules immobilized on the surfaces of the two above nanocrescents. A self-assembled monolayer of 3-mercaptopropyltrimethoxysilane (MTMO), a thiol-group containing molecule, is attached to the surface of the nanocrescents through Au sulfide bonds by spreading and drying a droplet of 1 μM MTMO in anhydrous ethanol solution. Figure 3c shows the SERS spectra of MTMO molecules on the background substrate and the nanocrescents in two different orientations. The spectra are taken using a laser excitation with 1 mW power and an integration time of 20 s. In accordance with the trend shown in the far-field scattering intensity measurement, it can be seen that the SERS enhancement factor of the perpendicularly oriented nanocrescent is higher than that of the obliquely oriented nanocrescent by comparing the intensity of 637 cm^{-1} Raman peak.

Since the orientation of suspended nanocrescents can be controlled dynamically by an external magnetic field, the SERS signal of MTMO molecules immobilized on the surface of a single nanocrescent can also be modulated magnetically. We prepared 1 μM MTMO-tethered nanocrescents suspended in 1 M ethanol solutions. The same magnet setup is used to apply the magnetic field. After the nanocrescents are stabilized under a constant magnetic field, the SERS spectra from a single nanocrescent are continuously taken while the orientation of the external magnetic field is changing. The integration time of spectra acquisition is 10 s, and every spectrum is taken after the magnet rotates for approximately 20°; the laser spot is tightly focused on the particle. Figure 3d shows the series of SERS spectra recorded as a function of time. The intensity of the 637 cm^{-1} Raman peak from MTMO molecules varies periodically and responds to the rotation of the permanent magnet. On the contrary, the intensities of the 864 and 1030 cm^{-1} peaks from the internal control, 1 M ethanol, remains relatively stable. It has been reported that solvent molecules, such as methanol and ethanol in water, will not be adsorbed on the substrate surface and not undergo the SERS effect;[12] therefore, the intensity of the Raman peaks from the solvent molecule can serve as an internal reference to calculate the Raman enhancement factor. Figure 3e shows the intensity of the 637 cm^{-1} peak versus the rotational angle of the permanent magnet. The illustrated peak intensities are normalized to the control peak intensities at 864 cm^{-1} in order to correct for laser-intensity fluctuations. The maximal SERS enhancement factor from the single nanocrescent at the perpendicular orientations is above 10^6 (1 M:1 μM) with respect to the internal control, and about seven times higher than that of the minimal enhancement from the nanocrescent at the oblique orientations. In fact, the enhancement factor could be even larger if only the number of target molecules adsorbed on the nanocrescent is compared with that of the solvent molecules present in the laser spot focal volume. The detectable volume of the solvent molecules is ~100 times larger than that of the adsorbed target molecules.[13] Therefore, the actual number of the target molecules can be 10^8 times smaller than that of the solvent molecules within the detectable focal volume, which results a Raman enhancement factor higher than eight orders of magnitudes and enables the detection of molecules at less than zeptomole concentrations. Since the Raman peak intensities of the solvent molecules, equivalent to a direct current signal, are constant, the signal-to-noise ratio of the SERS detection (an alternating current signal) can be improved through magnetic modulation, which is especially important when the Raman peaks from a complex background are as high as those of the tethered target molecules.

We demonstrate only one particular size of the multilayer composite nanocrescent SERS probes for the sake of clarity and consistency throughout this communication. In fact, the size, shape, and layer thickness can all be individually controlled by modifying the size of the sacrificial nanosphere template, the deposition angle, the deposited layer thickness, and the material of each layer. Since the plasmon-resonance wavelength of the metallic nanostructures is dependent on these parameters, the optical properties of the nanocrescent are tunable in our fabrication process. More studies on the optical properties of nanocrescents are underway. The Raman enhancement factor of a single nanocrescent is as high as those reported for nanoparticle clusters, and it is suitable for high-resolution biomolecular sensing in living cells. Furthermore, it can be precisely manipulated with proper magnetic-field control. The biocompatible Au surface can also be functionalized by tethering oligonucleotides, peptides, or antibodies using well-established methods.[14] The nanocrescents respond to near-infrared excitation, which has deeper penetration and results in less photothermal damage to cell tissue. Because of the above reasons, the biochemical composition of the local intracellular environment at the nanometer scale can potentially be measured by the translocation of standalone magnetic nanocrescent SERS probes to a desired position within living cells and detecting the fingerprints of biomolecules dynamically. The orientation modulation of nanocrescents by magnetic fields can further increase the signal-to-noise ratio in the dynamic SERS detections.

ADVANCED MATERIALS

Experimental

Sample Preparation: A thin layer of photoresist (Shipley S1818, Shipley, MA) was spin-coated on cleaned glass substrates. A monolayer of sacrificial nanospheres was generated by drop-casting a 0.1 % solution of polystyrene colloids (150 nm; Duke Scientific, CA), which was allowed to dry overnight in a clean-zone hood to minimize contamination of the samples by dust and to stabilize the rate of evaporation. After the arrays of beads dried, metal films in various thicknesses were deposited by conventional electron-beam evaporation. The sample substrate was placed above the metal-pellet sources with a certain tilt angle (~60°) with respect to the substrate surface. The substrate was rotated at a constant speed (~60 revolutions per minute, rpm) during the deposition. The metal-coated colloids were released from the glass support into an aqueous suspension by lift-off with acetone. Next, the coated polymer nanospheres were collected by centrifugation (~5000 rpm, 5–10 min) and suspended in toluene to dissolve the polystyrene. The sample was then centrifuged and washed three to four times in water. The nanocrescents were collected and resuspended in water or ethanol to form diluted colloids.

Fluorescence Imaging and Raman Microspectroscopy: A microscopy system combining fluorescence imaging and Raman spectroscopy was used to monitor the fluorescence intensity and to acquire Raman-scattering spectra from single nanocrescents. The system consisted of a Carl Zeiss Axiovert 200 inverted microscope (Carl Zeiss, Germany) equipped with a high-speed, high-sensitivity digital camera (Cascade 512B, Roper Scientific, NJ), and a 300 mm focal length monochromator (Acton Research, MA) with a 1024 pixel × 256 pixel cooled spectrograph charge-coupled device (CCD) camera (Roper Scientific, NJ). The time-resolved fluorescence images of the nanocrescents were taken using the Cascade camera at a frame rate of 10 frames per second, a 40× objective lens (numerical aperture NA = 0.8), a fluorescein isothiocyanate (FITC) fluorescence filter set, and a 100 W mercury lamp for illumination. A 785 nm semiconductor laser was used in our experiments as the excitation source of Raman scattering, and the laser beam was focused by a 100× objective lens on the nanocrescent. The excitation power was measured by a photometer (Newport, CA) to be ~1 mW. The Raman scattering light was then collected through the same optical pathway through a long-pass filter and analyzed by the spectrometer.

Received: May 25, 2005
Final version: August 1, 2005
Published online: September 29, 2005

[1] C. V. Raman, *Nature* **1928**, *121*, 619.
[2] Y. S. Huang, T. Karashima, M. Yamamoto, T. Ogura, H. Hamaguchi, *J. Raman Spectrosc.* **2004**, *35*, 525.
[3] M. Fleischm, P. J. Hendra, A. J. Mcquilla, *Chem. Phys. Lett.* **1974**, *26*, 163.
[4] S. M. Nie, S. R. Emery, *Science* **1997**, *275*, 1102.
[5] K. Kneipp, Y. Wang, H. Kneipp, L. T. Perelman, I. Itzkan, R. Dasari, M. S. Feld, *Phys. Rev. Lett.* **1997**, *78*, 1667.
[6] K. Kneipp, A. S. Haka, H. Kneipp, K. Badizadegan, N. Yoshizawa, C. Boone, K. E. Shafer-Peltier, J. T. Motz, R. R. Dasari, M. S. Feld, *Appl. Spectrosc.* **2002**, *56*, 150.
[7] Y. Lu, G. L. Liu, J. Kim, Y. X. Mejia, L. P. Lee, *Nano Lett.* **2005**, *5*, 119.
[8] S. J. Oldenburg, S. L. Westcott, R. D. Averitt, N. J. Halas, *J. Chem. Phys.* **1999**, *111*, 4729.
[9] A. Hartschuh, E. J. Sanchez, X. S. Xie, L. Novotny, *Phys. Rev. Lett.* **2003**, *90*, 095 503.
[10] J. Aizpurua, P. Hanarp, D. S. Sutherland, M. Kall, G. W. Bryant, F. J. G. de Abajo, *Phys. Rev. Lett.* **2003**, *90*, 057 401.
[11] J. N. Anker, R. Kopelman, *Appl. Phys. Lett.* **2003**, *82*, 1102.
[12] K. Kneipp, H. Kneipp, R. Manoharan, E. B. Hanlon, I. Itzkan, R. R. Dasari, M. S. Feld, *Appl. Spectrosc.* **1998**, *52*, 1493.
[13] The focal volume can be approximated as the volume of the cylindrical beam waist whose radius $r = 0.5$ μm and length $h = 5$ μm, that is, $\pi r^2 h = \pi(0.5)^2 \cdot 5$ μm$^3 \approx 3.8$ μm^3, while the volume of the single nanocrescent is about $4/3\pi(0.2)^3$ μm$^3 \approx 0.038$ μm^3.
[14] Y. W. C. Cao, R. C. Jin, C. A. Mirkin, *Science* **2002**, *297*, 1536.

A Highly Transparent and Luminescent Hybrid Based on the Copolymerization of Surfactant-Encapsulated Polyoxometalate and Methyl Methacrylate**

By *Haolong Li*, *Wei Qi*, *Wen Li*, *Hang Sun*, *Weifeng Bu*, and *Lixin Wu**

Polyoxometalates (POMs) are discrete, molecularly defined inorganic metal oxide clusters with dimensions ranging from approximately one to several nanometers. Their architectures not only exhibit a wide variety of topologies and compositions, but also lead to chemical, physical, and electronic versatility.[1] These specific properties give POMs potential applications in catalysis,[1b] optics,[2a] semiconductors,[2b] magnetics,[2c] and energy storage.[2d] However, in contrast to their intriguing functionality, practical POM-based materials or devices are quite limited. One of the important reasons for this is the inherent limitations, such as the poor processibility of pure POMs as inorganic crystalline or powdered materials. So, the development of suitable methods and technologies to protect and utilize POMs has become a focus topic in the application of POMs.

Several methods for manipulating and organizing POMs based on supramolecular assembly have proven to be effective and convenient, by which the POMs were fabricated into various matrices, such as inorganic silica networks,[3a] silica surfaces,[3b] organic surfactant systems,[3c–3e] and even liquid-crystal systems,[3f] etc. Although these systems have exhibited significant performance in different fields, polymer materials are another kind of promising matrix for the fabrication of POM-based materials because of their good stability and flexible processibility. Successful examples that use polymer ma-

[*] Prof. L. Wu, H. Li, W. Qi, W. Li, H. Sun, Dr. W. Bu
Key Laboratory for Supramolecular Structure and Materials of Ministry of Education
Jilin University, Changchun 130012 (P.R. China)
E-mail: wulx@jlu.edu.cn

[**] This work was supported by the National Natural Science Foundation of China (No. 20473032), the Major State Basic Research Development Program (No. G2000078102), the PCSIRT of Ministry of Education of China, and the Innovation Fund of Jilin University. We thank Mr. Fenghai Li for his help on the design of the molds. Supporting Information is available online from Wiley InterScience or from the author.

  DOI: 10.1002/adma.200500893